Determination of structural disorder in superionic Ag_2Te by neutron total scattering

1998 J. Phys.: Condens. Matter 10 8217

(http://iopscience.iop.org/0953-8984/10/37/009)

J. Phys.: Condens. Matter **10** (1998) 8217–8234. Printed in the UK PII: S0953-8984(98)94864-0

Determination of structural disorder in superionic Ag_2Te by neutron total scattering

David A Keen and Stephen Hull
ISIS Facility, Rutherford Appleton Laboratory, Chilton, Didcot, Oxon OX11 0QX, UK

Received 8 June 1998

Abstract. The structural disorder in the two high-temperature, superionic phases of Ag_2Te has been fully characterized using neutron powder diffraction and two complementary analyses. Rietveld profile refinement of Bragg scattering has been used to determine the most probable average structures and radial distribution functions, determined by Fourier transformation of the total scattering structure factors, have been used to refine local structural models based on these average structures. It is found that the α-phase, which exists between 420 K and 1075 K is best described by a face-centred cubic arrangement of the tellurium ions with the silver ions randomly occupying the tetrahedral and octahedral voids. There is no local ordering of the filled tetrahedral sites and the silver ions in octahedral sites have a broad distribution and preferentially sit off centre in one of the eight $\langle 111 \rangle$ directions away from filled tetrahedra. The γ-phase, which exists between 1075 K and the melt, has a body-centred cubic structure similar to α-AgI, and the average structure is best described with silver ions distributed over tetrahedral and trigonal sites and positions which join these two sites. The radial distribution functions in both superionic phases clearly show that silver ions are never closer than $\sim$2.4 Å to each other which means that nearest neighbour 12*d* tetrahedral sites cannot be simultaneously filled in γ-Ag_2Te. The differences in quality of fit to the experimental data between different silver ion ordering schemes are slight and it is proposed that single crystal diffuse scattering may be the only way to distinguish clearly between different models.

1. Introduction

Ag_2Te possesses two superionic phases at elevated temperature—the face-centred cubic (fcc) α-phase (420 K $< T <$ 1075 K) [1, 2] and the body-centred cubic (bcc) γ-phase (1075 K $< T <$ 1223 K) [2]. These two phases are isostructural with disordered superionic phases commonly found in the copper and silver halides, although with twice the number of cations filling the interstices formed by the anion sublattice. Our recent structural work [3] on the 'simple' binary copper and silver halides (where the superionic phases are characterized by rapid hopping of the cations between the interstitial sites formed by an essentially rigid anion sublattice) has shown that the anion sublattice is fcc in α-CuI and AgI-III and bcc in α-AgI, α-CuBr, CuCl-III and CuI-VII (the phases denoted by Roman numerals occur at high pressure). We conclude that there is an overwhelming preference for the cations to hop between tetrahedral sites. The absence of cations on octahedral sites (with the exception of AgI-III, which only becomes a good conductor when the tetrahedral sites become populated) is in contrast to EXAFS studies [4] but in accord with recent molecular dynamics work [5]. Since Ag_2Te has twice as many cations per formula unit as

0953-8984/98/378217+18$19.50

the equivalent halides it might be argued that the local arrangements within these disordered structures would have a greater tendency to order. If the ideal ordered anti-fluorite structure was realized for α-Ag_2Te and, by analogy with the superionic halides, conduction did not involve the octahedral sites, the ionic conduction would be hampered by the completely filled tetrahedral sites. Instead it is found that the ionic conductivity is extremely high in the α- and γ-phases with values of $\sim 1\ \Omega^{-1}\ cm^{-1}$ at 450 K rising to $\sim 6\ \Omega^{-1}\ cm^{-1}$ in the γ-phase [6]. In addition to the superionic properties of Ag_2Te, it is also a narrow bandgap semiconductor and calculations of the electronic properties require an accurate structural description (see, for example, [7]).

There have been several investigations of the structure of Ag_2Te (e.g., [1, 2, 8]), the most comprehensive of which is by Schneider and Schulz [2]. Freuh [8] correctly determined the room temperature monoclinic structure of β-Ag_2Te in space group $P2_1/c$. The structure of the α-phase was initially described in space group $F\bar{4}3m$ [9], but later work assigned the structure to $Fm\bar{3}m$ [1]. The debate concerning the structure of this phase relates to the locations of the cations in the tetrahedral and octahedral sites and how they disorder between these sites. Comparing [1] and [2] shows that there is not a clear consensus. The γ-phase was shown to have a bcc anion sublattice by Freuh [10] who proposed a random arrangement of cations with this sublattice. Subsequent work [2] has distributed the cations randomly between 12*d* sites in space group $Im\bar{3}m$, following the earlier determinations of the structure of α-AgI [11].

This paper sets out to address possible local ordering schemes in Ag_2Te using time-of-flight neutron total scattering measurements from powdered samples. It has been shown (e.g., [12, 13]) that by using the total scattering to refine an average structural model it is possible to deduce local disorder in crystalline materials. The advantage of this method over more conventional crystallographic interpretations of structural disorder is that total scattering probes the correlations between pairs of atoms at an instant of time, whereas Bragg (or elastic) scattering determines the time-averaged distribution of scattering density within the unit cell. Therefore, in contrast to previous studies, it is possible to deduce local correlations between atoms which reside, on average, on partially-filled sites.

2. Experimental details

A powdered Ag_2Te sample from the Johnson Matthey chemical company was loaded into a cylindrical silica ampoule of 6 mm internal diameter and 0.75 mm wall thickness and sealed under vacuum. The ampoule, in a thin-walled vanadium can, was placed inside a furnace with a vanadium heating element and heat shields. Measurements of the time-of-flight neutron total scattering were made on the POLARIS powder diffractometer [14] at the ISIS spallation neutron source collecting data from all four detector banks which are centred at 14°, 35°, 90° and 145°. In all, measurements were made from the sample at a number of temperatures covering the three phases of Ag_2Te which exist above room temperature as well as measurements of a vanadium standard rod, empty furnace and empty silica ampoule. The empty silica ampoule was measured at similar temperatures to those of the sample since the structured scattering at high-Q from silica is strongly temperature dependent [15].

Data from the $\sim 90°$ detector banks were corrected in the standard manner (instrumental background subtraction only and including absorption corrections) for Rietveld profile refinement [16]. This bank collects data which are a good compromise between resolution and long d-spacing reflections. Time-of-flight Rietveld refinements of the powder diffraction data used the computer programme TF14LS [17]. In assessing the relative quality of fits to

the experimental data using different structural models the usual χ^2 statistic is used, defined by

$$\chi^2 = \sum_{N_d} \frac{(I_{obs} - I_{calc})^2}{(\sigma I_{obs})^2} \Big/ (N_d - N_p). \tag{1}$$

N_d is the number of data points used in the fit and N_p is the number of fitted parameters. I_{obs} and I_{calc} are the observed and calculated intensities, respectively, and σI_{obs} is the estimated standard deviation on I_{obs}, derived from the counting statistics.

In addition, data from all four detector banks were corrected for container and furnace background, absorption, multiple scattering and inelasticity effects in an identical manner to that routinely used for liquid or amorphous scattering [18] to obtain the fully corrected, total scattering structure factors $F(Q)$ on an absolute scale. $F(Q)$ contains the Bragg and diffuse scattering, and can be cast in terms of the total radial distribution function $G(r)$:

$$F(Q) = \rho \int_0^\infty 4\pi r^2 G(r) \frac{\sin(Qr)}{Qr}\, \mathrm{d}r \tag{2}$$

where

$$G(r) = \sum_{i=1}^{n} \sum_{j=1}^{n} c_i c_j \bar{b}_i \bar{b}_j [g_{ij}(r) - 1] \tag{3}$$

and c_i and $\bar{b}_i$ are the proportion and neutron scattering length of atom type i, respectively, and $g_{ij}(r)$ are the partial radial distribution functions which correlate the distance atoms j are from atoms i at an instant of time.

3. Results

3.1. Average structures

Figure 1 shows the comparison between data collected at $2\theta \sim 90^\circ$ in all three phases and the Rietveld fitted 'best' models. Good fits were obtained in all cases. Although previous measurements [1, 2] have incorporated anharmonic terms in their structural models, all the models shown here use isotropic temperature factors only. Where disordering is seen to occur, this is characterized by using a partially-filled 'split-site' model of the disorder. Data measured below 150 °C confirmed the structure of Hessite, β-Ag_2Te (see table 1). This structure is composed of distorted $AgTe_4$ tetrahedra and is described in detail in [19]. There is no occupancy of octahedral sites in this structure.

Table 1. Structural parameters for β-Ag_2Te at 60 °C. B_{iso} is the isotropic temperature factor.

β-Ag_2Te at 60 °C, space group $P2_1/c$, $\chi^2 = 0.926$, $a = 8.159(4)$ Å, $b = 4.4820(2)$ Å, $c = 8.977(3)$ Å, $\beta = 123.96(1)^\circ$.				
Atom	x	y	z	B_{iso} (Å^2)
Te	0.2749(7)	0.166(2)	0.2423(8)	1.4(1)
Ag1	0.025(1)	0.156(2)	0.375(1)	2.0(1)
Ag2	0.327(1)	0.844(2)	0.997(1)	4.4(2)

Table 2. Different structural models of the average cation disorder in α-Ag_2Te at 200 °C. B_{iso} is the isotropic temperature factor and SITE is the number of cations distributed within the symmetry related sites. F denotes a parameter which was not varied during the refinement.

α-Ag_2Te at 200 °C, $a = 6.6128(1)$ Å, space group $Fm\bar{3}m$, Te in 4*a* at (000) etc, Ag1 in tetrahedral site, Ag2 in octahedral site									
			Te	Ag1			Ag2		
	Model	χ^2	B_{iso} (Å^2)	B_{iso} (Å^2)	x	SITE	B_{iso} (Å^2)	x	SITE
1	Ag1 in 8*c* ($\frac{1}{4}\ \frac{1}{4}\ \frac{1}{4}$)	2.308	6.2(2)	10.3(2)		8.0(F)			
2	Ag1 in 8*c* ($\frac{1}{4}\ \frac{1}{4}\ \frac{1}{4}$)	1.921	7.7(3)	8.8(2)		6.5(2)			
3	Ag1 in 32*f* ($x\ x\ x$)	1.821	8.0(3)	3.5(4)	0.286(1)	6.4(1)			
4	Ag1 in 8*c* ($\frac{1}{4}\ \frac{1}{4}\ \frac{1}{4}$) Ag2 in 4*b* ($\frac{1}{2}\ \frac{1}{2}\ \frac{1}{2}$)	1.402	11.1(2)	7.2(1)		4.0(F)	60(2)		4.0(F)
5	Ag1 in 8*c* ($\frac{1}{4}\ \frac{1}{4}\ \frac{1}{4}$) Ag2 in 4*b* ($\frac{1}{2}\ \frac{1}{2}\ \frac{1}{2}$)	1.403	10.9(3)	7.3(2)		4.1(2)	49(2)		3.9(2)
6	Ag1 in 8*c* ($\frac{1}{4}\ \frac{1}{4}\ \frac{1}{4}$) Ag2 in 48*i* ($x\ x\ \frac{1}{2}$)	1.389	11.3(4)	7.3(3)		4.2(3)	27(3)	0.394(3)	3.8(3)
7	Ag1 in 8*c* ($\frac{1}{4}\ \frac{1}{4}\ \frac{1}{4}$) Ag2 in 32*f* ($x\ x\ x$)	1.311	9.9(3)	7.6(2)		5.1(2)	14(2)	0.406(1)	2.9(2)

3.1.1. α-Ag_2Te. Table 2 shows a number of models for the cation disordered structures of α-Ag_2Te at 200 °C, all in space group $Fm\bar{3}m$. Model $\alpha 1$ is the ideal anti-fluorite structure with the cations filling the tetrahedral interstices formed by the anion sublattice. Model $\alpha 2$ is identical to $\alpha 1$, except that the occupancy of the cation site has been allowed to vary. A reduced value of χ^2 is obtained with only 6.5 of the possible eight cations remaining on the tetrahedral 8*c* site, clearly showing that the cations are disordering from this site, but not giving any indication of where they are disordering to. Model $\alpha 3$ mimics the effect of anharmonicity on the tetrahedral site by splitting each 8*c* ($\frac{1}{4}\ \frac{1}{4}\ \frac{1}{4}$) cation site into four 32*f* ($x\ x\ x$) sites each $\frac{1}{4}$ occupied. Models $\alpha 4$ to $\alpha 7$ all contain additional cation disorder, whereby the octahedral interstices become occupied, either on the ideal 4b ($\frac{1}{2}\ \frac{1}{2}\ \frac{1}{2}$) site ($\alpha 4, \alpha 5$) or further disordered within the octahedral voids ($\alpha 6, \alpha 7$). As models $\alpha 4$ to $\alpha 7$ show (and in contrast to related halide structures, such as α-CuI [20]), good fits are only obtained when cations are placed in octahedral as well as tetrahedral sites, although as models $\alpha 4$ and $\alpha 5$ indicate, the isotropic temperature factors of cations in the octahedral sites are very large. Further disordering of the cations within this site using split-site models produces small improvements in χ^2. Model $\alpha 7$, with cations distributed between sites away from ($\frac{1}{2}\ \frac{1}{2}\ \frac{1}{2}$) in $\langle x\ x\ x\rangle$ directions (as suggested by [1]) with $x = 0.406(1)$ produces a better fit than model $\alpha 6$, where the cations are distributed between ($x\ x\ \frac{1}{2}$) positions (as preferred by [2]) with $x = 0.394(3)$. For completeness, one further model was tested in space group $F\bar{4}3m$ with Te in 4*a* at (0 0 0) and Ag in 4*c* at ($\frac{1}{4}\ \frac{1}{4}\ \frac{1}{4}$) and 4*b* at ($\frac{1}{2}\ \frac{1}{2}\ \frac{1}{2}$). This is equivalent to the model first proposed by Rahlfs [9] and it gave a χ^2 of 2.891 with isotropic temperature factors of 6.8(2), 10.5(1) and 54(2) Å^2 for Te and Ag in 4*c* and 4*b*, respectively. This agreement with the data is inferior to all the models outlined above and it is concluded that $Fm\bar{3}m$ is the correct space group for α-Ag_2Te.

Model $\alpha 7$ is therefore the preferred average structural model for this phase, not only because of the marginally smaller value of χ^2, but also because it has a more realistic Ag^2

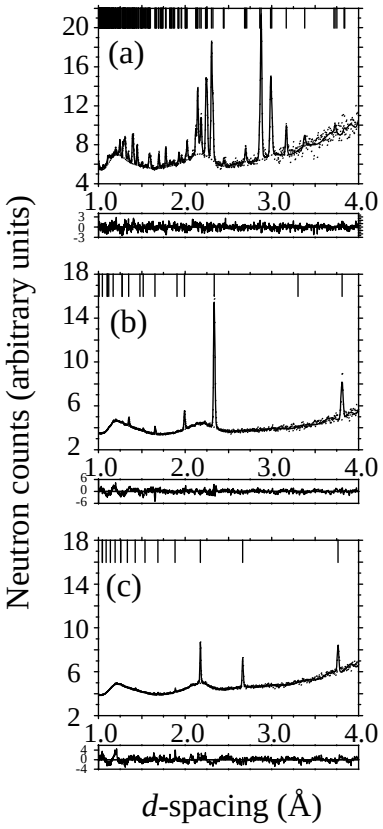

Figure 1. Least-squares refinement of the diffraction data from Ag_2Te at (a) 60 °C (β-phase), (b) 200 °C (α-phase) and (c) 800 °C (γ-phase). The dots are the experimental points and the full line is the profile calculated using the 'best' structural model for each phase as described in the text. The tick marks at the top of each main panel show the calculated positions of the Bragg peaks and the smaller panels show the difference (measured minus calculated) divided by the estimated standard deviation of the data points.

temperature factor and the disordering is towards the faces of the octahedron, rather than the octahedron edges. Although model $\alpha 7$ has a significant number of cations in the octahedral interstices, consideration of the 32*f* position and temperature factor shows that the ideal octahedral site may actually be a minimum in the cation density (see figure 2) and further confirms the model for ionic conduction [5] in these fcc structures, whereby cations jump in skewed ⟨100⟩ directions between nearest-neighbour tetrahedral sites via the peripheries of the octahedral interstices.

3.1.2. γ-Ag_2Te. Similar cation-disordered models of the γ-phase at 800 °C are shown in table 3. Taking three possible sites for the cation within the bcc framework of anions (octahedral 6*b* (model $\gamma 1$), tetrahedral 12*d* (model $\gamma 2$) and trigonal 24*h* (model $\gamma 3$)) [11] separately, the 12*d* and 24*h* sites are clearly preferred over the octahedral 6*b* sites. Model $\gamma 4$ is a random combination of 12*d* and 24*h* sites. This produces a very slight improvement in χ^2, with slightly more cations on 12*d* sites than 24*h* sites, but this is no better than a simple random distribution of cations from the 12*d* sites into neighbouring 48*i* sites with

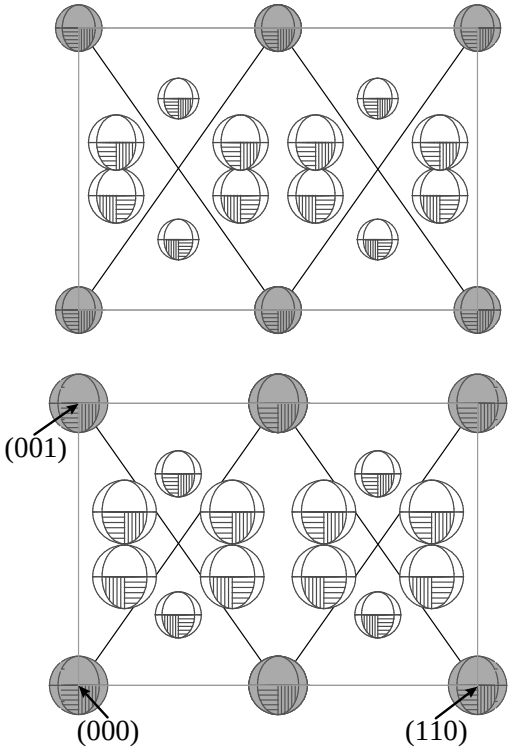

Figure 2. The average structure of α-Ag_2Te at 200 °C (upper plot) and 700 °C (lower plot) showing anions (shaded) and cations (unshaded). Plots show the thermal ellipsoids at the 50% probability level for all atoms in a (110) section through the unit cell. The diagonal lines indicate the positions of the boundaries between tetrahedral and octahedral interstices.

$(\frac{1}{4}, x, \frac{1}{2} - x)$ and $x = 0.046(3)$ (model $\gamma 5$). The $12d \rightarrow 48i$ splitting is equivalent to preferentially spreading the cation density on the $12d$ sites in the four directions towards the $8c$ sites. Since only small changes in χ^2 are observed for the differently disordered structural models $\gamma 2$, $\gamma 3$, $\gamma 4$ and $\gamma 5$, on the basis of the Bragg scattering the structure may be best described as a bcc arrangement of anions surrounded by a continuum of cations which are distributed evenly between tetrahedral and trigonal sites and positions which join the two.

Figure 3 shows the volume per Ag_2Te formula unit at all the temperatures measured. There is a ∼3.9% volume expansion on going from the β- to the α-phase whereas on passing from the α- to the γ-phase the volume is almost unchanged or may even decrease slightly. A similar small decrease in cell volume is observed on passing from fcc α-CuI to bcc CuI-VIII with increasing temperature at high pressure [21]. The volume increases linearly in the α-phase. Refining data at different temperatures using model $\alpha 7$ for the α-phase shows that there is nothing anomalous in the temperature behaviour in this phase; the temperature factors increase with increasing temperature, the average position of the $32f$ octahedral site moves further away from its ideal $(\frac{1}{2}\ \frac{1}{2}\ \frac{1}{2})$ position and the cation occupancy of the tetrahedral and octahedral sites remains constant at all temperatures (with ∼5.33 cations in the tetrahedral sites). These results compare well with measurements of the linear expansion of β- and α-Ag_2Te [22] which give a 4.0% change in volume at the β–α transition and

Table 3. Different structural models of the average cation disorder in γ-Ag_2Te at 800 °C. B_{iso} is the isotropic temperature factor and SITE is the number of cations distributed within the symmetry related sites.

γ-Ag_2Te at 800 °C, $a = 5.3323(1)$ Å, space group $Im\bar{3}m$, Te in 2*a* at (000) etc								
			Te	Ag1		Ag2		
	Model	χ^2	B_{iso} (Å^2)	B_{iso} (Å^2)	SITE	B_{iso} (Å^2)	x	SITE
1	Ag1 in 6*b* ($\frac{1}{2}\ \frac{1}{2}\ 0$)	3.531	9.4(3)	60(2)	4.0(F)			
2	Ag1 in 12*d* ($\frac{1}{4}\ 0\ \frac{1}{2}$)	1.502	11.8(3)	22.2(7)	4.0(F)			
3	Ag2 in 24*h* ($x\ x\ 0$)	1.537	13.8(4)			17.8(6)	0.356(1)	4.0(F)
4	Ag1 in 12*d* ($\frac{1}{4}\ 0\ \frac{1}{2}$) Ag2 in 24*h* ($x\ x\ 0$)	1.445	12.4(4)	19(1)	2.3(4)	=Ag1 B_{iso}	0.345(6)	1.7(5)
5	Ag2 in 48*i* ($\frac{1}{4}, x, \frac{1}{2} - x$)	1.452	13.0(4)			20.1(6)	0.046(3)	4.0(F)

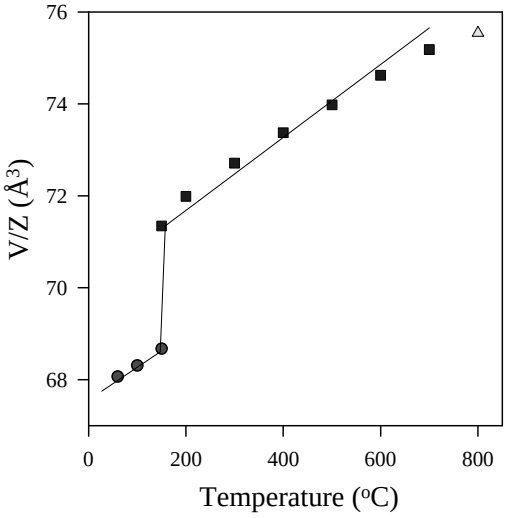

Figure 3. Volume per Ag_2Te formula unit at a number of temperatures. Circles correspond to the β-phase, squares to the α-phase and the triangle to the γ-phase. In all cases the errors are smaller than the size of the symbols. Superimposed on the data are lines corresponding to the linear expansion data of Honma and Iida [22], referenced to the volume of β-Ag_2Te at 295 K [19].

a thermal expansion coefficient of 2.47×10^{-5} K^{-1} and 3.57×10^{-5} K^{-1} for the β- and α-phases, respectively.

Before turning our attention to the local ordering schemes within these structures it should be emphasized that the α-phase is face-centred cubic over the whole temperature range. There is no evidence for a tetragonal structure which has been observed by others between 419 K and 533 K [23] and used to interpret more recent conductivity measurements [24].

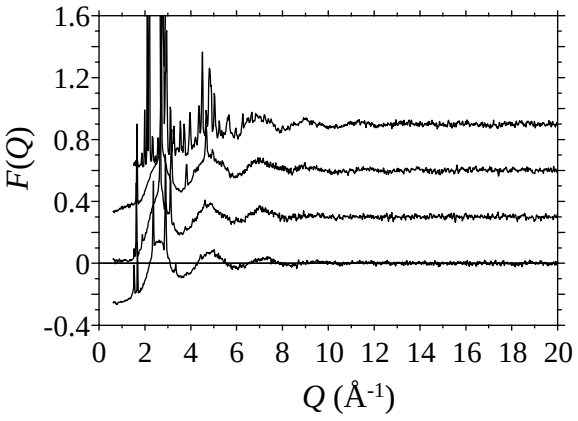

Figure 4. Total scattering structure factors for β-Ag_2Te at 60 °C (uppermost curve), α-Ag_2Te at 200 °C and 700 °C and for γ-Ag_2Te at 800 °C (lowest curve). Each successive curve has been offset vertically by 0.3 for clarity. (There is a weak Bragg peak at low-Q in γ-Ag_2Te which probably originates from slight sample decomposition.)

3.2. Local structures

Experimental total scattering structure factors $F(Q)$ are shown for the three phases of Ag_2Te in figure 4. The two high-temperature phases show substantial diffuse scattering and only weak Bragg peaks. Whereas the long-range structure changes significantly on going from the α- to the γ-phase, with a change from fcc to bcc anion arrangements, the diffuse scattering from these two phases appears qualitatively similar. The radial distribution functions $G(r)$ of α-Ag_2Te at 200 °C and α-Ag_2Te at 800 °C, obtained by Fourier transforming the data in figure 4 (see equation (2)), are shown as dashed curves in the top panels of figures 5 and 6, respectively. The first significant peak occurs at ∼2.85 Å in both phases which is predominantly due to the nearest-neighbour Ag–Te distance when the cation resides in the tetrahedral sites of both structures. This peak is much weaker in the γ-phase than in the α-phase, but it has the same width. There is also an indication of a slight asymmetry in the peak shape in the α-phase, with it being sharper on the low-r side. There are no peaks at lower r values which means that there are no atom–atom correlations shorter than ∼2.4 Å which discounts simultaneous cation occupation of nearest-neighbour 12*d* tetrahedral sites in γ-Ag_2Te, but does not restrict possible local orderings in the α-phase. There is little structure in $G(r)$ beyond this first peak in γ-Ag_2Te, and any small-amplitude oscillation is out of phase with the high-r oscillations in the $G(r)$ of α-Ag_2Te. The Ag–Ag and Ag–Te correlations dominate the neutron weighted $G(r)$ (see equation (3)—$c_i c_j \bar{b}_i \bar{b}_j$ is 0.156 for Ag–Ag, 0.153 for Ag–Te + Te–Ag and 0.037 for Te–Te). Hence the weak long-range oscillations in $G(r)$ for γ-Ag_2Te only suggests a very disordered or 'liquid-like' distribution of *cations*. The *anions* which dictate the crystalline lattice are primarily seen in the Te–Te correlations. These only contribute around 10% to $G(r)$ and may still possess long-range order.

Various models have been constructed in order to understand further the local ordering of the cations within these two disordered structures. It is possible to use total scattering data to refine an average structure model with the reverse Monte Carlo (RMC) method [25]. Briefly, a configuration of N atoms is created from $n_x \times n_y \times n_z$ unit cells of a given average crystal structure. These atoms are moved randomly one at a time, and under periodic boundary conditions and after each move the correlations are compared with the measured

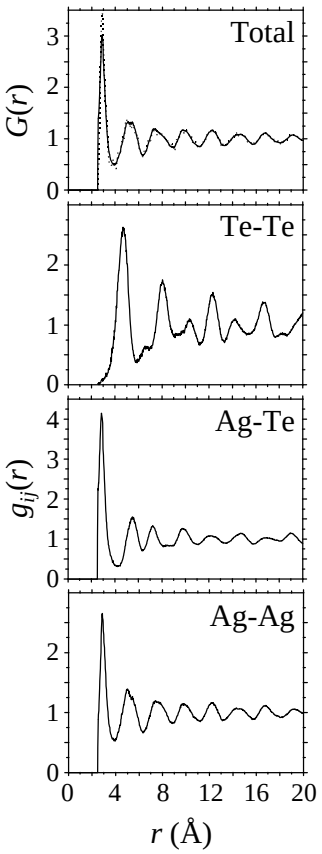

Figure 5. Radial distribution functions $G(r)$ and $g_{ij}(r)$ for α-Ag_2Te at 200 °C obtained from the converged RMC model and fitting to $F(Q)$ (see text for details). The dashed curve in the uppermost plot is the experimental $G(r)$ obtained from the direct Fourier transform of $F(Q)$.

data (either $G(r)$, for comparison in real space or $F(Q)$, for comparison in reciprocal space) using the following function:

$$\chi^2_{RMC} = \sum (F_{calc}(Q_i) - F_{expt}(Q_i))^2/\sigma(Q_i)^2 + \chi^2_{constraints} \tag{4}$$

summing over all i points, each with estimated error σ and substituting $G(r)$ for $F(Q)$ when appropriate. The final term on the right-hand side allows the incorporation of constraints to force the models to have specific characteristics (such as specific coordinations, bondlengths, angles etc). In this particular instance, we restricted the possible moves of the anions to be always less than 0.025 Å. This has the effect of keeping the crystalline lattice intact without recourse to further constraints. Atom moves are accepted or rejected on the basis of the change in χ^2_{RMC}. If χ^2_{RMC} is smaller after the move, the move is accepted and if χ^2_{RMC} is larger then the move is accepted with a probability $\exp(-\Delta\chi^2/2)$ in a manner analogous to the standard Monte Carlo simulation method [26]. The refinement is said to have converged when further moves give, on average, no improvement to χ^2_{RMC}.

3.2.1. Modelling the local structure of α-Ag_2Te. Three starting models for the α-phase were constructed. Each model was a cubic configuration of $8 \times 8 \times 8$ unit cells under

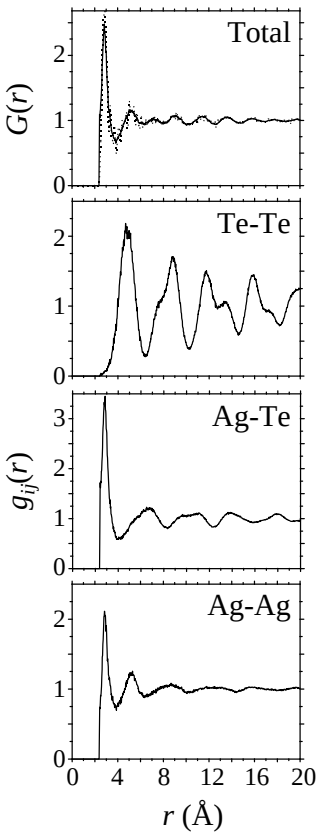

Figure 6. Radial distribution functions $G(r)$ and $g_{ij}(r)$ for γ-Ag_2Te at 800 °C obtained from the converged RMC model and fitting to $F(Q)$ (see text for details). The dashed curve in the uppermost plot is the experimental $G(r)$ obtained from the direct Fourier transform of $F(Q)$.

periodic boundary conditions. The first consisted of the anti-fluorite structure whereby all tetrahedral sites were filled with cations and the octahedral sites were empty. The second had half the tetrahedral sites filled in an arrangement analogous to the zinc-blende structure, whereby first-neighbour tetrahedral sites (separated by $(\frac{1}{2}\,0\,0)$ etc) could not be simultaneously occupied, and completely-filled octahedral sites (the structure proposed by Rahlfs [9]). The third model had a random filling of octahedral and tetrahedral sites resulting in 5.333 cations in tetrahedral sites and 2.667 in octahedral sites. Atoms were all initially placed on ideal sites. To begin with, all models were refined for the same fixed amount of time, fitting to either $G(r)$ or $F(Q)$ from α-Ag_2Te at 200 °C and changing the positions of the cations by less than 0.05 Å in each step. After this time χ^2_{RMC} was compared and the refined models examined. The short time and small moves kept the cations within their starting anion interstices. After approximately 1 000 000 generated moves (570 000 accepted moves), χ^2_{RMC} was 35 for model 1, 38 for model 2 and 11 for model 3 when fitting to $F(Q)$ with $\sigma = 0.005$. Model 3 also gave the lowest χ^2_{RMC} when fitting to $G(r)$. This shows that occupation of octahedral sites and nearest-neighbour tetrahedral sites are both necessary in order to reproduce the local correlations. If every unit cell in the model is collapsed onto one single unit cell, it is possible to relate this local model to the average structure. It is found that the anion density is distributed isotropically and centred on its

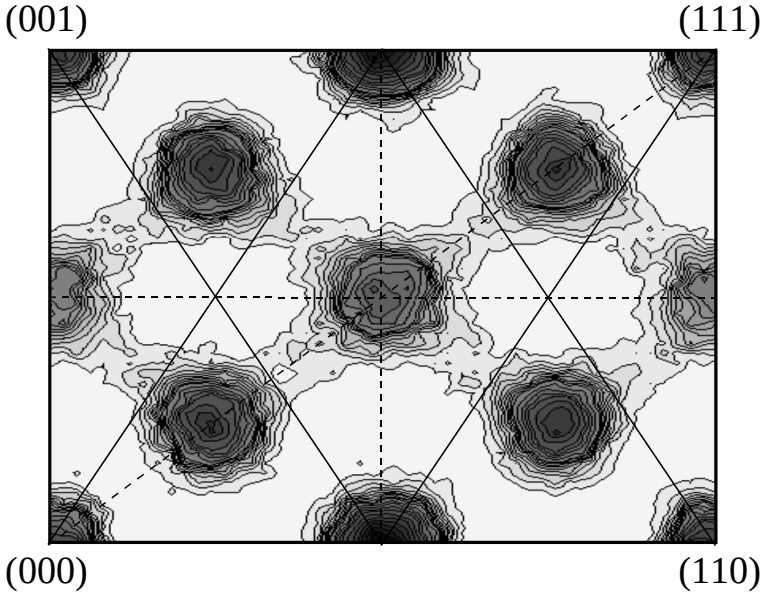

Figure 7. Distribution of ion density in γ-Ag_2Te at 800 °C within a (x x z) section of the unit cell. Anions are at the top and bottom of the plot and all other contours are cation density. The full lines indicate the positions of the boundaries between tetrahedral and octahedral interstices and the dashed lines indicate the directions of the density cuts shown in figure 8. The plot has been obtained from averaging over independent converged RMC configurations fitting to $F(Q)$ (see text for details).

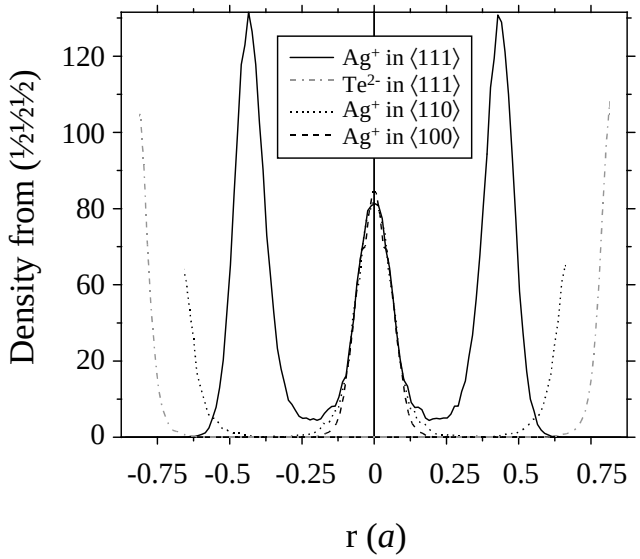

Figure 8. Ion density within the unit cell of α-Ag_2Te at 200 °C in various directions from $(\frac{1}{2}\ \frac{1}{2}\ \frac{1}{2})$. The density has been obtained from averaging over independent converged RMC configurations fitting to $F(Q)$ (see text for details).

lattice site, whereas the distribution of cations is anisotropic. The distribution around the octahedral site is broad, spreading most in the ⟨111⟩ directions and the distribution around

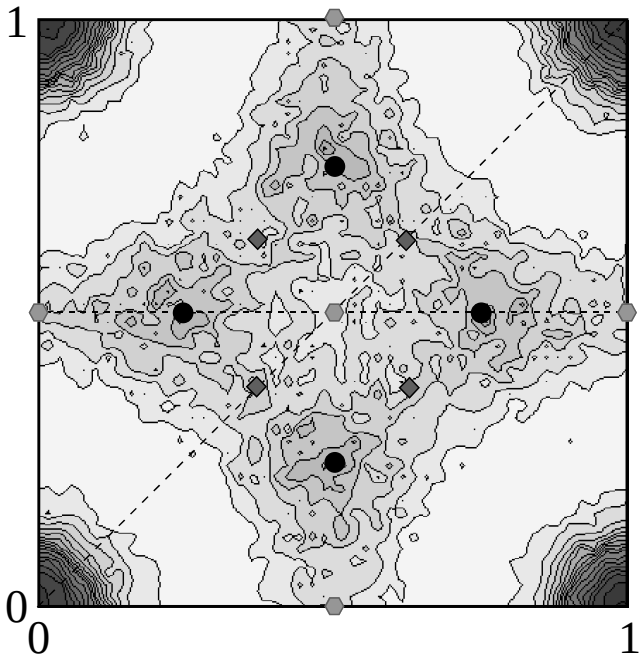

Figure 9. Distribution of ion density of γ-Ag_2Te at 800 °C within a (x y 0) section of the unit cell. Anions are at the four corners of the plot and all other contours are cation density. The dashed lines indicate the directions of the density cuts shown in figure 10. Full circles, diamonds and hexagons show the positions of the 12*d* tetrahedral, 24*h* trigonal and 6*b* octahedral sites, respectively. The plot has been obtained from averaging over independent converged RMC configurations fitting to $F(Q)$ (see text for details).

the tetrahedral sites is peaked at the ideal ($\frac{1}{4}$ $\frac{1}{4}$ $\frac{1}{4}$) etc positions, but with some spread in ⟨111⟩ directions away from the neighbouring anions. In model 2, with a zinc-blende filling of the tetrahedral sites, the octahedral site density was asymmetric with a clear preference for the octahedral cation to move away from neighbouring filled tetrahedral sites.

Subsequently, the anti-fluorite structure was refined using RMC until the calculated $F(Q)$ from the model had converged fully to the experimental $F(Q)$ from α-Ag_2Te at 200 °C. This time larger (<0.2 Å) cation moves were used and the Ag atoms were allowed to move between possible interstices. The radial distribution functions from this refinement are shown in figure 5. There is good agreement between the total $G(r)$ calculated from the RMC configuration and $G(r)$ obtained from direct Fourier transformation of the experimental $F(Q)$. Figures 7 and 8 show the distribution of ion density in a (110) section and in various directions about ($\frac{1}{2}$ $\frac{1}{2}$ $\frac{1}{2}$) in the unit cell, respectively. Although the starting configuration only had cations in tetrahedral ($r = \pm 0.433a$ in figure 8) interstices, the converged configuration possesses cations in both tetrahedral and octahedral ($r = 0$) interstices in a proportion consistent with random filling. In addition, the tetrahedral and octahedral sites are joined in ⟨111⟩ directions by a region of non-zero density, whereas the density does not spread so far from the centre of the octahedral site in either the ⟨110⟩ or ⟨100⟩ directions.

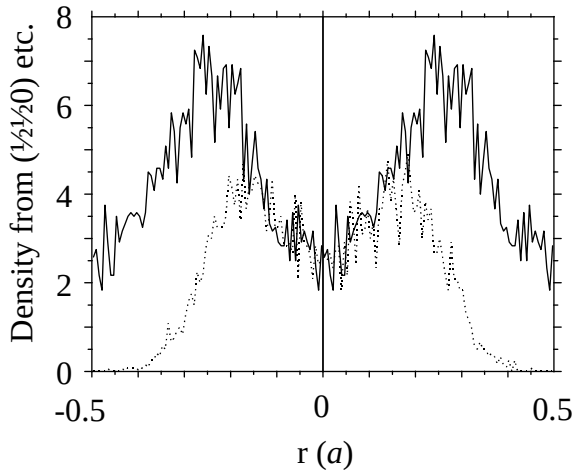

Figure 10. Cation density within the unit cell of γ-Ag_2Te at 800 °C in ⟨100⟩ (full curve) and ⟨110⟩ directions (dotted curve) from the 6*b* octahedral sites at $(\frac{1}{2}\ \frac{1}{2}\ 0)$ etc. The density has been obtained from averaging over independent converged RMC configurations fitting to $F(Q)$ (see text for details).

3.2.2. Modelling the local structure of γ-Ag_2Te. Similarly, three starting models for γ-Ag_2Te at 800 °C were constructed from $10 \times 10 \times 10$ unit cells, based on random cation filling of octahedral, tetrahedral or trigonal sites with the additional requirement that no two ions were less than 2.4 Å apart. The same refinement protocol was used for each of these simulations as for α-Ag_2Te. After a fixed amount of time, each simulation resulted in approximately the same value of χ^2_{RMC} and substantial disorder of the cations was found in all three cases. The disorder was such as to move the cations away from the starting octahedral sites and to join the trigonal sites to the tetrahedral sites. In other words, the tetrahedral starting model disordered towards the trigonal sites and *vice versa*. The anion density remained isotropic and peaked at its lattice site for all the models.

Finally, a configuration based on the tetrahedral sites was refined to $F(Q)$ from γ-Ag_2Te at 800 °C using the RMC method and larger (<0.2 Å) Ag atoms moves until convergence. The radial distribution functions from this refinement are shown in figure 6. Again there is good agreement between the total $G(r)$ calculated from the RMC configuration and $G(r)$ obtained from direct Fourier transformation of the experimental $F(Q)$. As expected, there is much less long-range structure in the $g_{Ag-Ag}(r)$ (which is almost flat beyond $r \sim 16$ Å) than $g_{Ag-Te}(r)$ or $g_{Te-Te}(r)$ or any of the equivalent functions from α-Ag_2Te at 200 °C (see figure 5). Figure 9 shows a contour plot of the $x = 0$ etc section of atom density within the unit cell of γ-Ag_2Te at 800 °C from the RMC converged configurations. The anions are distributed isotropically around the four (symmetry-related) corners of the plot at 2*a* (000), whereas the cations atoms are distributed more widely, peaking at the tetrahedral 12*d* $(\frac{1}{4}\ 0\ \frac{1}{2})$ sites, but spreading towards the 'ideal' trigonal 24*h* sites. There is some occupation of the octahedral 6*b* sites, but this is a density minimum. Figure 10 shows two cuts through this distribution in the ⟨100⟩ and ⟨110⟩ directions, both centred on the 6b octahedral site at $(\frac{1}{2}\ \frac{1}{2}\ 0)$. This figure shows that the positions of the peaks in cation density are at the tetrahedral ($r = \pm 0.25a$ in the figure) and 'ideal' trigonal ($r = \pm 0.177a$) in the ⟨100⟩ and ⟨110⟩ directions, respectively.

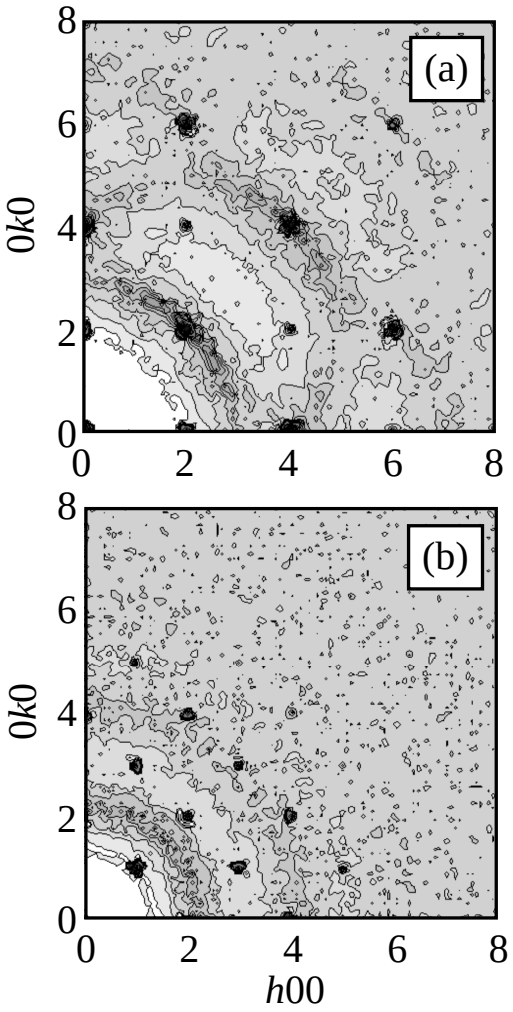

Figure 11. Diffuse scattering in the $hk0$ reciprocal lattice plane calculated from the converged RMC model of (a) α-Ag_2Te at 200 °C and (b) γ-Ag_2Te at 800 °C (see text for details).

4. Discussion

4.1. Comparison between local and average structures

The local structures deduced by RMC refinement of total scattering data and the average structures determined from Rietveld refinement of the Bragg intensities should be consistent. In general this is the case; α-Ag_2Te has the tetrahedral and octahedral interstices of the anion sublattice randomly filled with cations in both the average and local structure models and the cation disorder is in the $\langle 111 \rangle$ directions. The local structure of γ-Ag_2Te places the cations in and around sites shown to be favourable in the average models. However, there are small differences. For example, figure 2 shows the average structure of α-Ag_2Te with the refined thermal ellipsoids for the atoms. This suggests a minimum in cation density at $(\frac{1}{2}\ \frac{1}{2}\ \frac{1}{2})$. Figures 7 and 8 show the cation density from the converged RMC refined local structure

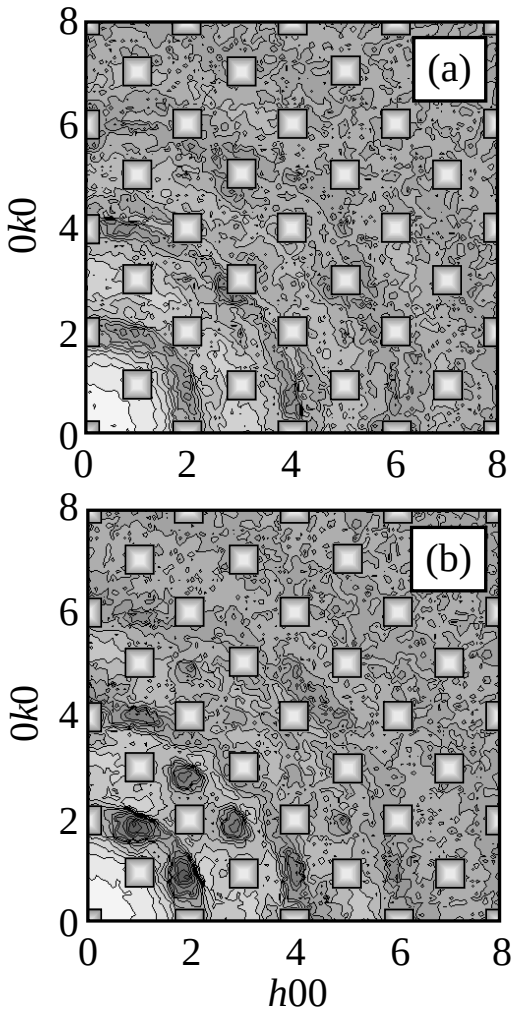

Figure 12. Diffuse scattering in the $hk0$ reciprocal lattice plane calculated from (a) the trigonal model and (b) the tetrahedral model of γ-Ag_2Te at 800 °C (see text for details). The shaded squares correspond to the positions of the Bragg peaks for this bcc structure. The same contour levels have been used in (a) and (b).

with a maximum at $(\frac{1}{2}\ \frac{1}{2}\ \frac{1}{2})$. The local structure refinement shows that there is considerable, presumably dynamic, disorder of the cations with continuous density between tetrahedral and octahedral interstices. It is not straightforward to envisage a simple average structural model which can account for such a complex distribution of cation density. Considering the small number of observable Bragg peaks, we have chosen to use split-site models with as few structural parameters as possible, although this may give a too simplistic average model. Schneider and Schultz [2] use a far more complicated split-site model and include anisotropic temperature factors in their models. They also suggest that the centre of the octahedral site is energetically unfavourable. RMC refinement is independent of potential functions and therefore cannot distinguish energetically unfavourable sites and the constraints of the data and an excluded volume (whereby ions may not overlap each other—in these refinements ions were not permitted to be closer than 2.4 Å to each other) do not preclude the occupation

of the centre of the octahedral sites. The best conclusion that can be drawn is that neither average nor local structure models are correct in all respects, largely due to the limited nature of the experimental data. A possible way forward is to use single crystal diffraction. This would separate the Bragg reflections of equivalent $h^2 + k^2 + l^2$ and allow the measurement of more Bragg intensities. It would also give a better picture of the diffuse scattering, since a powder average of the diffuse scattering does not directly distinguish between isotropic (i.e. only varying as $|\boldsymbol{Q}|$) diffuse features and diffuse features which are $\boldsymbol{Q}$-dependent.

Figure 11 shows the diffuse scattering in the $hk0$ reciprocal lattice plane calculated from ten independent converged RMC configurations for (a) α-Ag_2Te at 200 °C and (b) γ-Ag_2Te at 800 °C. The calculated diffuse scattering for α-Ag_2Te is strongly structured in $\boldsymbol{Q}$ and broad diffuse peaks spread from strong $hh0$ reflections towards symmetry forbidden $hk0$ (e.g. 310, 530 etc). In contrast, the diffuse scattering for γ-Ag_2Te consists of two broad rings of scattering at $|\boldsymbol{Q}|$-values consistent with the diffuse peaks in $F(Q)$ (see figure 4). Similar plots were calculated for the models of α-Ag_2Te and γ-Ag_2Te which had been refined for a fixed amount of time with small atom moves. It was found that the diffuse scattering from these models of α-Ag_2Te was very similar in all cases, but that the intensities of the weaker Bragg reflections were different for different models. In contrast, the diffuse scattering in the γ-phase was very different for the different models. Figure 12 shows the diffuse scattering in the $hk0$ reciprocal lattice plane calculated from 10 independent configurations starting from trigonal sites (figure 12(a)) and from tetrahedral sites (figure 12(b)). Here the diffuse scattering from the two models is significantly different with strongly peaked scattering under 210, 230 etc in the tetrahedral model and more isotropic scattering in the trigonal model. Clearly, measurement of the single crystal diffraction patterns of these two disordered phases would give data which are more sensitive to the various structural models. However, it is not straightforward to perform such a measurement, particularly with neutrons, since large single crystals may not survive the first-order nature of the phase transitions at high temperature. It may be possible to grow large single crystals *in situ* from the melt (as has been done for α-AgI [27]).

4.2. Comparison of local structures with other related systems

There are several other materials which possess related high-temperature disordered superionic phases, some of which (e.g. AgI [28], CuI [29] and CuBr [30]) have been investigated using RMC methods. In addition, there have been several molecular dynamics (MD) simulations of CuI [5] and Ag_2Te [31]. α-CuBr and α-AgI are isostructural to γ-Ag_2Te and α-CuI to α-Ag_2Te. The partial radial distribution functions for γ-Ag_2Te are very similar to those determined using RMC for α-CuBr and α-AgI, although the $g_{ij}(r)$ in [28] possess more structure since they were determined at a lower temperature. The low-r peak in $g_{Ag-Ag}(r)$ is stronger in γ-Ag_2Te, since Ag_2Te has twice the number of cations than either CuBr or AgI. This is also seen in the relative occupations of the tetrahedral, trigonal and octahedral sites, where there are relatively more cations in the octahedral sites in γ-Ag_2Te than in α-CuBr or α-AgI. However, the $g_{ij}(r)$ determined using RMC are different for α-Ag_2Te and α-CuI since α-CuI does not have a significant cation occupation of octahedral sites and hence Cu–Cu correlations of $(\sqrt{3}/2)a$ are largely absent in α-CuI. Finally, MD simulations of α-Ag_2Te show a broad distribution of cation density, centred on the tetrahedral site and spreading smoothly to the octahedral site. There is no peak at the octahedral site, although the overall occupation of the octahedral interstices is high.

5. Conclusions

The structural disorder in Ag_2Te at high temperature has been characterized using a combination of Rietveld refinement of neutron powder diffraction and RMC modelling of neutron total scattering. The two high-temperature structures both show considerable disorder of the diffusing cations. In α-Ag_2Te the cations occupy the tetrahedral and octahedral interstices within the fcc anion sublattice, although there is still some ambiguity in the manner in which the cations occupy the octahedral site. Good fits to the total scattering are only obtained when nearest-neighbour tetrahedral sites and octahedral sites are simultaneously filled. The various models produced from RMC refinement of total scattering show little differences in diffuse scattering but significant differences in the intensities of the weak Bragg intensities which are not observed in the powder diffraction. γ-Ag_2Te has a bcc arrangement of anions and the cations are preferentially distributed between the tetrahedral and trigonal sites and the regions between them. The RMC models produced from refining the total scattering in this phase do not conclusively differentiate between possible preferred sites, although the $\boldsymbol{Q}$-dependent diffuse scattering calculated from each model is significantly different.

Although one should be cautious in inferring too much from such poorly constrained local structural models, it does suggest that only by carrying out a careful single crystal study, collecting both the Bragg intensities and diffuse scattering can a clearer picture of the structural disorder of these two high-temperature phases of Ag_2Te be obtained.

References

[1] Sakuma T and Saitoh S 1985 *J. Phys. Soc. Japan* **54** 3647
[2] Schneider J and Schulz H 1993 *Z. Kristallogr.* **201** 1
[3] Hull S and Keen D A 1994 *Phys. Rev.* B **50** 5868–85
Hull S and Keen D A 1996 *J. Phys.: Condens. Matter* **8** 6191–8
Keen D A, Hull S, Hayes W and Gardner N J G 1996 *Phys. Rev. Lett.* **77** 4914–17
[4] Boyce J B and Huberman B A 1979 *Phys. Rep.* **51** 189
[5] Zheng-Johansson J X M, Ebbsjo I and McGreevy R L 1995 *Solid State Ionics* **82** 115
[6] Miyatini S 1981 *J. Phys. Soc. Japan* **50** 3415
[7] Kikuchi H, Iyetomi H and Hasegawa A 1997 *J. Phys.: Condens. Matter* **9** 6031–48
[8] Freuh A J 1959 *Z. Kristallogr.* **112** 44–52
[9] Rahlfs P 1936 *Z. Phys. Chem.* B **31** 57–194
[10] Freuh A J 1961 *Am Mineral.* **46** 654–60
[11] Wright A F and Fender B E F 1977 *J. Phys. C: Solid State Phys.* **10** 2261
[12] Keen D A 1998 *Local Structure from Diffraction* ed S J L Billinge and M F Thorpe (New York: Plenum) pp 101–20
[13] Keen D A, McGreevy R L, Hayes W and Clausen K N 1990 *Phil. Mag. Lett.* **61** 349–57
Keen D A, Hayes W and McGreevy R L 1990 *J. Phys.: Condens. Matter* **2** 2773–86
Nield V M, Keen D A, Hayes W and McGreevy R L 1992 *J. Phys.: Condens. Matter* **4** 6703–14
[14] Hull S, Smith R I, David W I F, Hannon A C, Mayers J and Cywinski R 1992 *Physica* B **180/181** 1000
[15] Susman S, Volin K J, Montague D G and Price D L 1991 *Phys. Rev.* B **43** 11 076–81
[16] Smith R I and Hull S 1997 *Rutherford Appleton Laboratory Report* RAL-TR-97-038
[17] David W I F, Ibberson R M and Matthewmann J C 1992 *Rutherford Appleton Laboratory Report* RAL-92-031
[18] Howe M A, McGreevy R L and Howells W S 1989 *J. Phys.: Condens. Matter* **1** 3433–51
[19] van der Lee A and de Boer J L 1993 *Acta Cryst.* C **49** 1444–6
[20] Keen D A and Hull S 1995 *J. Phys.: Condens. Matter* **7** 5793–804
[21] Hull S and Keen D A 1997 Private communication
[22] Honma K and Iida K 1987 *J. Phys. Soc. Japan* **56** 1828
[23] Izumi Y and Miyatani S 1973 *J. Phys. Soc. Japan* **35** 312
[24] Rom I and Sitte W 1994 *Solid State Ionics* **70/71** 147–52

[25] Keen D A 1997 *Phase Transitions* **61** 109–24
McGreevy R L and Pusztai L 1988 *Mol. Simulation* **1** 359
[26] Binder K and Heermann D W 1992 *Monte Carlo Simulation in Statistical Physics—An Introduction* 2nd edn (Berlin: Springer)
[27] Keen D A, Nield V M and McGreevy R L 1994 *J. Appl. Cryst.* **27** 393–8
[28] Nield V M, Keen D A, Hayes W and McGreevy R L 1993 *Solid State Ionics* **66** 247–58
[29] Chahid A and McGreevy R L 1998 *J. Phys.: Condens. Matter* **10** 2597–609
[30] Nield V M, McGreevy R L, Keen D A and Hayes W 1994 *Physica* B **202** 159–66
[31] Tachibana F, Kobayashi M and Okazaki H 1988 *Solid State Ionics* **28–30** 41–5
Shimojo F and Okazaki H 1992 *J. Phys. Soc. Japan* **61** 4465–73